Top Quark Mass Measurement in the 2 fb^{-1} Tight Lepton and Isolated Track Sample using Neutrino ϕ Weighting Method

Igor Suslov[1], Marco Trovato[2], Vladimir Glagolev[1], George Velev[3], Oleg Pukhov[1], Giorgio Bellettini[2], Julian Budagov[1], Guram Chlachidze[1,3], Alexei Sissakian[1]

We report on a measurement of the top quark mass in the lepton + track sample using **Neutrino ϕ Weighting Method (PHI)** at the statistics close to 2 fb^{-1}. This method was already successfull aplied twice to the CDF II data: at the statistics 190 pb^{-1} [1] and later on at the statistics 340 pb^{-1} [2]. The last result was published at PRD[3].

1 Principles of the Method

1.1 Constrained variables

We have unconstrained kinematic situation for the "PHI" method: a total number of 24 unknown (b, $\overline{b}$, l^-, l^+, ν, $\overline{\nu}$ 4-momenta) and only 23 equations (measured 3-momenta for two b-jets and two leptons, assumed knowing mass for 6 final particles, used two transverse component of calorimeter missing energy, constrained invariant mass for two W and assumed equal constrained mass of top and antitop quarks) to use to constrain the kinematics.

Obviously, it is impossible to pick up directly only one solution per event. We must assume some of the event parameters ($\vec{R}$); as known, in order to constrain the kinematics and then vary the $\vec{R}$ to determine the variety of solutions. In addition, every solution must have a weight attached to it.

[1]JINR, Dubna

[2]INFN and Department of Physics, University of Pisa

[3]Fermilab

The minimal requirement in the case of $-1C$ kinematics to perform the χ^2 minimization is to use a two dimensional vector as $\vec{R}$. For our analysis we chose the azimuthal angles of the neutrino momenta $\vec{R} = (\phi_{\nu 1}, \phi_{\nu 2})$ and we create a net of solutions in the $(\phi_{\nu 1}, \phi_{\nu 2})$ plane.

1.2 Fitter procedure

In this section we will clarify the idea about the tool, called "Fitter". The "Fitter" receives as input a set of information about a selected event and gives at output one reconstructed top quark mass per event.

1.2.1 The χ^2 form

The **Fitter** uses final particles momentum, jet energy information as well as constrain on W ant t masses. The common formula for χ^2 is:

$$\chi^2 \equiv -2ln(\mathscr{P}(\mathbf{x})) \tag{1}$$

where $\mathbf{x}$ is a general notation to indicate a variable and $\mathscr{P}$ its probability density distribution. The expanded formula of χ^2 is :

$$\begin{aligned}
\chi^2 &= \chi^2_{reso} + \chi^2_{constr} \qquad (2)\\
\chi^2_{reso} &= \sum_{l=1}^{2} \frac{(P_T^l - \tilde{P_T^l})^2}{{\sigma^l_{P_T}}^2} + \sum_{j=1}^{2}[-2ln(\mathscr{P}_{tf}(\tilde{P_T^j}|P_T^j))] + \sum_{i=x,y} \frac{(UE^i - \tilde{UE^i})^2}{{\sigma^i_{UE}}^2}\\
\chi^2_{constr} &= -2ln(\mathscr{P}_{BW}(m_{inv}^{l_1,\,\nu_1}|M_W,\,\Gamma_{M_W})) - 2ln(\mathscr{P}_{BW}(m_{inv}^{l_2,\,\nu_2}|M_W,\,\Gamma_{M_W})) +\\
&\quad -2ln(\mathscr{P}_{BW}(m_{inv}^{l_1,\,\nu_1,j_1}|\tilde{M}_t,\,\Gamma_{\tilde{M}_t}) - 2ln(\mathscr{P}_{BW}(m_{inv}^{l_2,\nu_2,j_1}|\tilde{M}_t,\,\Gamma_{\tilde{M}_t}))
\end{aligned}$$

The variables with a tilde sign refer to the output of the minimization procedure, whereas P_T and UE (unclustered energy) represent measured values corrected for known detector and physics effects. $\tilde{M}_t$ is the fit parameter giving the reconstructed top mass. BW and tf are for the relativistic Breit-Wigner and transfer function respectively. Notice that we splitted the χ^2 into two parts: the first one, χ^2_{reso}, takes into account the detector uncertainties, whereas the second one deals with the known mass constraints.
The first sum runs over the primary lepton (tight lepton) and the track lepton. We use the known expressions for a calorimeter and a tracker for the uncertainty in measuring primary electron and muon P_T respectively. For the track lepton we

use the same formula as for the muons:

$$\frac{\sigma^e_{P_T}}{P^e_T} = \sqrt{\frac{a}{P^e_T} + b} \tag{3}$$

$$\frac{\sigma^\mu_{P_T}}{P^\mu_T} = c \cdot P^\mu_T \tag{4}$$

where $a = 0.135^2$, $b = 0.02^2$, $c = 0.0011$ are taken from the Run I study [4].

The second sum is over the two leading jets. These transverse momenta have been further corrected for multiple interactions, underlying event and out-of-cone energy (level 6 and 7), even though only level-5 corrected jets were considered for selection purposes.

The third sum is over the two transverse components of the unclustered energy[1]. The other term in the formula (2), χ^2_{reso}, refers to the invariant masses of the couples lepton-neutrino and of the lepton-neutrino-leading jet system. We set $M_W = 80.41 GeV/c^2$, $\Gamma_{M_W} = 2.06 GeV/c^2$, as suggested by P.D.G., and we insert the function Γ_{M_t} (see Figure 1), according to the standard model [5].

The insertion of the top width dependence from the top mass is something new: we will dedicate a subsection at the end of this section to point out the changes and the improvements obtained by introducing this new characteristic in the Fitter.

1.2.2 Scanning of the $(\phi_1, \ \phi_2)$ plane

We should integrate over the subvariety spanned by the constraining variables: we choose a step and we scan all the $(0, 2\pi) \times (0, 2\pi)$ (ϕ_1, ϕ_2) net according to it.
For each point of the net we can write the following linear system:

$$\begin{cases} P_T^{\nu_1} cos(\phi_{\nu_1}) \ + \ P_T^{\nu_2} cos(\phi_{\nu_2}) \ = \ \not{E}_{T_x} \\ P_T^{\nu_1} sin(\phi_{\nu_1}) \ + \ P_T^{\nu_2} sin(\phi_{\nu_2}) \ = \ \not{E}_{T_y} \end{cases} \tag{5}$$

[1] UE is defined as the sum of all unclustered energy in the calorimeter, that is the sum of all the towers which are not associated with any of the objects previously considered in the χ^2 formula (tight lepton, track-lepton, two leading jets): notice that this definition also includes remaining jets with $E_T > 8 \ GeV$ and $|Eta| < 2$ that are not already taken into account as leading jets.

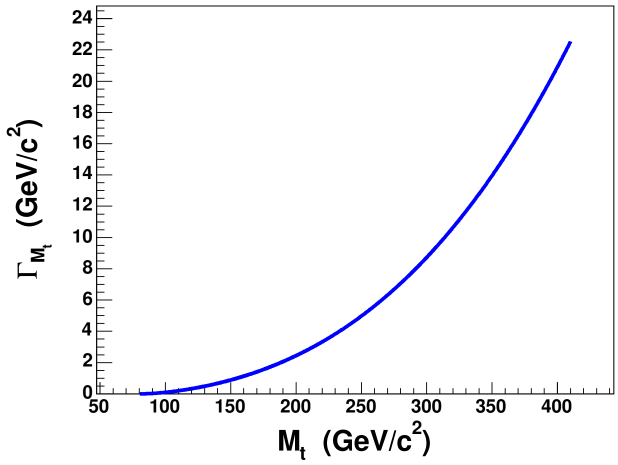

Figure 1: Top Width Vs top mass

that is solved by:

$$\begin{cases} P_x^{\nu 1} \equiv P_T^{\nu 1} \cdot cos(\phi_{\nu 1}) = \frac{\not{E}_x \cdot sin(\phi_{\nu 2}) - \not{E}_y \cdot cos(\phi_{\nu 2})}{sin(\phi_{\nu 2} - \phi_{\nu 1})} \cdot cos(\phi_{\nu 1}) \\ P_y^{\nu 1} \equiv P_T^{\nu 1} \cdot sin(\phi_{\nu 1}) = \frac{\not{E}_x \cdot sin(\phi_{\nu 2}) - \not{E}_y \cdot cos(\phi_{\nu 2})}{sin(\phi_{\nu 2} - \phi_{\nu 1})} \cdot sin(\phi_{\nu 1}) \\ P_x^{\nu 2} \equiv P_T^{\nu 2} \cdot cos(\phi_{\nu 2}) = \frac{\not{E}_x \cdot sin(\phi_{\nu 1}) - \not{E}_y \cdot cos(\phi_{\nu 1})}{sin(\phi_{\nu 1} - \phi_{\nu 2})} \cdot cos(\phi_{\nu 2}) \\ P_y^{\nu 2} \equiv P_T^{\nu 2} \cdot sin(\phi_{\nu 2}) = \frac{\not{E}_x \cdot sin(\phi_{\nu 1}) - \not{E}_y \cdot cos(\phi_{\nu 1})}{sin(\phi_{\nu 1} - \phi_{\nu 2})} \cdot sin(\phi_{\nu 2}) \end{cases} \tag{6}$$

Since we add two additional values, we perform a *1C* fit minimization of the χ^2 (2). This is done for every point of the net, with a particular attention to avoid those ones satisfying the equation $\phi_{\nu_1} - \phi_{\nu_1} = k \cdot \pi$ with $k = 0, 1$ (in practice there is no limitation because we optimize the net by avoiding these points).

We must notice that we would have the same components of the neutrino 's momentum $P_{x,y}^{\nu_1,\ \nu_2}$ for $\phi'_{\nu 1, \nu 2} = \phi_{\nu 1, \nu 2} + \pi$ (see 6) and we would take into accounts three unphysical solutions ($P_T^{\nu 1} < 0$ and/or $P_T^{\nu 2} < 0$). We subdivide the whole net we should scan $(0, 2\pi) \times (0, 2\pi)$ into a 4 areas: $(0, \pi) \times (0, \pi)$, $(0, \pi) \times (\pi, 2\pi)$, $(\pi, 2\pi) \times (0, \pi)$, $(\pi, 2\pi) \times (\pi, 2\pi)$.

We stay away from the unwelcome inconvenience by scanning a $(0, \pi)(0, \pi)$ net and by changing sign to $P_T^{\nu 1, \nu 2}$ in the case we find unphysical solutions and automatically change the phi quadrant as shown by the equation below:

$$\phi'_{\nu1,\nu2} = \phi_{\nu1,\nu2} + \pi \implies p'^{\,\nu1,\nu2}_{x,y} = p^{\nu1,\nu2}_{x,y} \text{ and } P'^{\,\nu1,\nu2}_{T} = -P^{\nu1,\nu2}_{T}$$

The net is chosen to have 12x12 points for $(0,\pi)\times(0,\pi)$ (ϕ_1,ϕ_2): the reason we do not choose a finer segmentation is because we do not see big profit in templates smearings, instead of we lose in CPU timing to get each solution ($\approx$ 30 msec per combination).

Starting from the 8 solutions per net point per event (longitudinal momentum component for every neutrino has two solution and there is a ambiguity in coupling W with b-jets) we can finally say that we have to do 1152 $1C$ minimizations which return the (M^{reco}_{ijk}) and χ^2_{ijk} $(i = 1,\ldots,12;\ j = 1,\ldots,12;\ k = 1,\ldots,8)$ at the output.

We select the lowest χ^2 with associated mass for every point of the (ϕ_1,ϕ_2) net, this way we reduce the number of obtained masses to 144. Each of these masses should be taken into account because each of them arise from a particular and physical configuration of our event: *the problem is how to establish the right weight for them.*

1.2.3 Weghting the solutions

In section 1.2.1 we apply the Breit-Wigner functions inside the χ^2 formula (2) for W and t invariant mass distributions. The relativistic Breit-Wigner formula is:

$$BW(m_{inv};\ m,\Gamma) \sim \frac{1}{(m^2_{inv} - m^2)^2 + m^2\Gamma^2} \tag{7}$$

For our analyses we decided to use the next Breit-Wigner normalization to obtain the top mass solutions:

$$BW(m_{inv};\ m,\Gamma) = \frac{\Gamma^2\cdot m^2}{(m^2_{inv} - m^2)^2 + m^2\Gamma^2} \tag{8}$$

where m and Γ are the mass and top width for t or W particles, depending on the considered decay chain; m_{inv} refers to the invariant mass, calculated with the appropriate information from lepton and neutrino, in the case of W decay, or lepton, neutrino and leading jet, in the case of t decay.

In the case of $W \to l\nu$ Breit-Wigner, formula (8) has a constant numerator, which has not any importance in the χ^2 minimization. Instead of Γ_t depends on of the parameter (top mass, see Figure 1) of the χ^2 minimization.

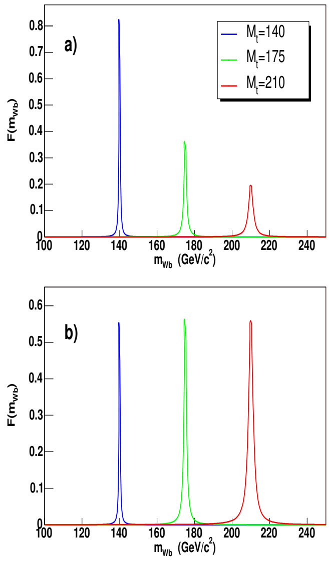

Figure 2: The relativistic Breit-Wigner functions: top - equation (9), bottom - equation(8)

Our investigation shows that the distribution of reconstructed mass has the smaller error and the more accurate mean value if we apply for the solution weights renormalized Breit-Wigner formula:

$$BW(m_{inv};\ m,\Gamma)\ =\ \frac{\Gamma\cdot m^2}{(m_{inv}^2\ -\ m^2)^2\ +\ m^2\Gamma^2} \tag{9}$$

This function is normalized to 1, instead of the previous one which has the maximum independent of the top mass: see Figure 2. We are using the χ^2 definition (according to (9)) to give a probability of occurence to our 144 solutions. The expression for the weight is given below:

$$w_{ij}\ =\ e^{-\frac{\chi^2_{ij}}{2}};\qquad i,j=1,\cdots,12 \tag{10}$$

this formula is obtained by inverting (1).

1.3 Picking up the solution

Once we have decided the weight for each of the 144 masses per event, we define an optimized procedure to obtain the final reconstructed mass per event. The procedure follows the steps below:

1. We build a probability density mass distribution by using χ^2_{ij} and (M^{reco}_{ij}) info: we will have 144 entries for all of the events.

2. We identify the MPV value.

3. We apply a cut on our probability density distribution (”pdd”): we decide to apply a discriminator level (DL) and we don’t consider in the calculation of the final average mass for the event (M^{reco}_t) all those masses that have a bin content less than the DL fraction of the MPV value.

4. At the end we calculate M^{reco}_t by performing a weighted average over all the masses that pass the step 3, according to the weight given in the formula (10).

In this measurement we are using **DL = 0.3**, which was optimized and described in the CDF internal note [2].

1.4 Likelihood Form

The likelihood function finds the probability that our data candidates are described by an appropriate admixture of background events and dilepton $t\bar{t}$ decays with a certain top quark mass.

We performe comparison by parametrizing the mass distributions in Monte Carlo, building a M^{reco}_T on the data sample and finally matching the two by using the likelihood unbinned fit and minimization.

The likelihood function has the following form:

$$\mathscr{L} = \mathscr{L}_{shape} \cdot \mathscr{L}_{backgr} \cdot \mathscr{L}_{param}; \tag{11}$$

where,

$$\mathscr{L}_{shape} = \frac{e^{-(n_s+n_b)} \cdot (n_s + n_b)^N}{N!} \cdot \prod_{n=1}^{N} \frac{n_s \cdot f_s(m_n|M_{top}) + n_b \cdot f_b(m_n)}{n_s + n_b} \tag{12}$$

and

$$\mathscr{L}_{backgr} = exp(\frac{-(n_b - n_b^{exp})^2}{2\sigma^2_{n_b}}) \tag{13}$$

$$\mathscr{L}_{param} = exp\{-0.5[(\vec{\alpha} - \vec{\alpha_0})^T U^{-1} (\vec{\alpha} - \vec{\alpha_0}) + (\vec{\beta} - \vec{\beta_0})^T V^{-1} (\vec{\beta} - \vec{\beta_0})]\}. \quad (14)$$

Here U and V are the covariance matrices for the parameters $\vec{\alpha_0}$ and $\vec{\beta_0}$ respectively.

The likelihood maximization procedure (we usually minimize $-ln(\mathscr{L})$) returns a **true top quark estimator** $\mathbf{m_t}$ and an estimated number of signal (n_s) and background (n_b). We assign a probability (f_s) that each of the selected "LTRK" event looks like signal and the probability (f_b) that this event can be considered as background one.

These two probabilities are weighted according to appropriate signal and background numbers, n_b and n_s, that, as we already wrote, are self-estimated by the likelihood fit. Anyway these two parameters are not completely free: the first one follows a Gaussian distribution (see 13) where n_b^{exp} and σ_{n_b} are taken from "LTRK" dilepton cross section group [7], while the $n_s + n_b$ is constrained by a Poisson term $\frac{e^{-(n_s+n_b)} \cdot (n_s+n_b)^N}{N!}$, as shown in 12. It should be notice that this way the likelihood estimated number of signal events is independent from the expected number of signal events calculated by using $t\bar{t}$ cross section info.

Moreover we want to point out that "PHI" method uncertainties in the signal and background parametrization are included directly into the statistical error estimation procedure.

2 PHI Method optimization

As mentioned above (section 1.2.1), in this section we are going to explain what are the improvements we obtained by upgrading the χ^2 in the formula (2) and the way of weighting the top mass solutions (see 10).

Basically we introduced two changes in the definition of the χ^2: we switched from the approximate gaussian functions of the previous analysis [2] to the more physical correct Breit-Wigner distributions, concerning to t, $\bar{t}$, $W^{\pm}$ decays, and we use the m_t dependendent Γ_t instead of the constant value used before [2].

We have compared the top mass spectra reconstructed by means of the slighty different functions for the Breit-Wigner (9) and (8) included in χ^2.

In Figure 3 the plots were built by using Monte Carlo information at parton level. Only one solution per event was picked up because we do not have any uncertainties about P_z^{ν}, (ϕ_1, ϕ_2) and lepton-jets pairings. Because of this reason this check is weight-indepent. Monte Carlo generated events with $M_t = 161, 171\ and 181\ GeV/c^2$ were used.

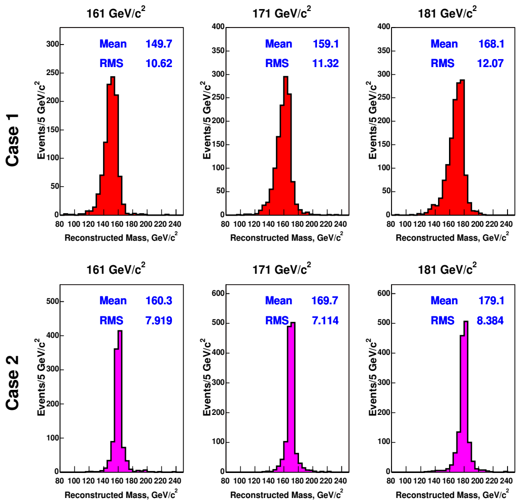

Figure 3: Top mass reconstruction at HEPG level by using Breihgt-Wigner (9) and (8)

The comparison shows the advantage of the function (8) applied for χ^2 minimization. As a next step of optimization we tried a different kind of weight applied to the top mass solutions.

We compared the different ways of reconstructing top invariant masses (see Figure 4):

- *Case 0*: Gaussian distribution function for both χ^2 and weight ([2]).
- *Case A*: Breit-Wigner's as in 8 for the χ^2 and its natural weight (10)
- *Case B*: Breit-Wigner's as in 9 for the χ^2 and its natural weight (10)
- *Case C*: Mixed combination: Breit-Wigner's as in (8) for the χ^2 and the weight recalculated according to Breit-Wigner functions (9).

In the Figure 4 we plotted the estimated statistical errors[2] calculated by using Monte Carlo generated $t\bar{t}$ events only and an expected number of signal events $n_s = 60.53$ [7], versus input top quark mass.

[2]This error is obtained by performing the pseudo experiments tecnique

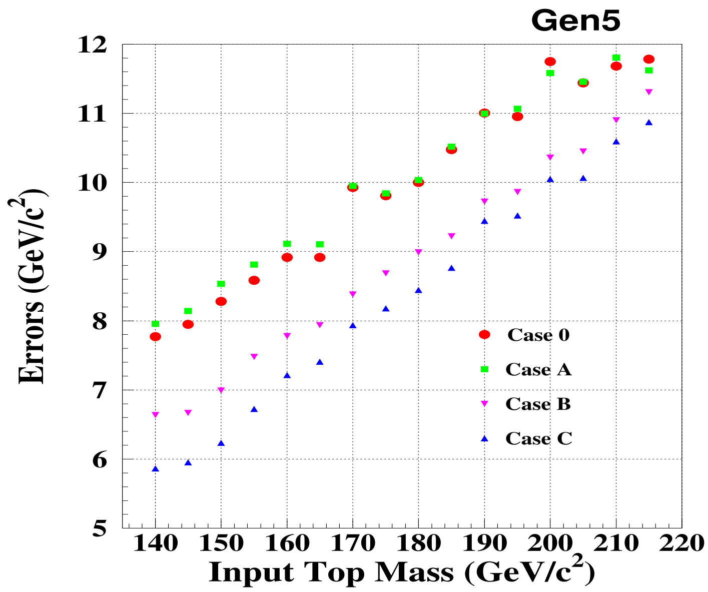

Figure 4: Improvements in final statistical errors by using m_t mass dependent, Breit-Wigner functions and two different weights for the top mass solutions

The conclusion is clear: **The method C** is chosen as our final way since it has the best resolution.

Moreover we changed the leading jet term inside the equation (2). We switched from the formula $\sum_{j=1}^{2} \frac{(P_T^j - \widetilde{P_T^j})^2}{{\sigma^j_{P_T}}^2}$ (j runs over the two leading jets) to one that exploit our transfer function[3].

Figure 5 represents the variable $k = (P_T^{part} - P_T^{jet})/P_T^{jet}$, fitted in different $(|\eta|, P_T^{jet})$ regions.

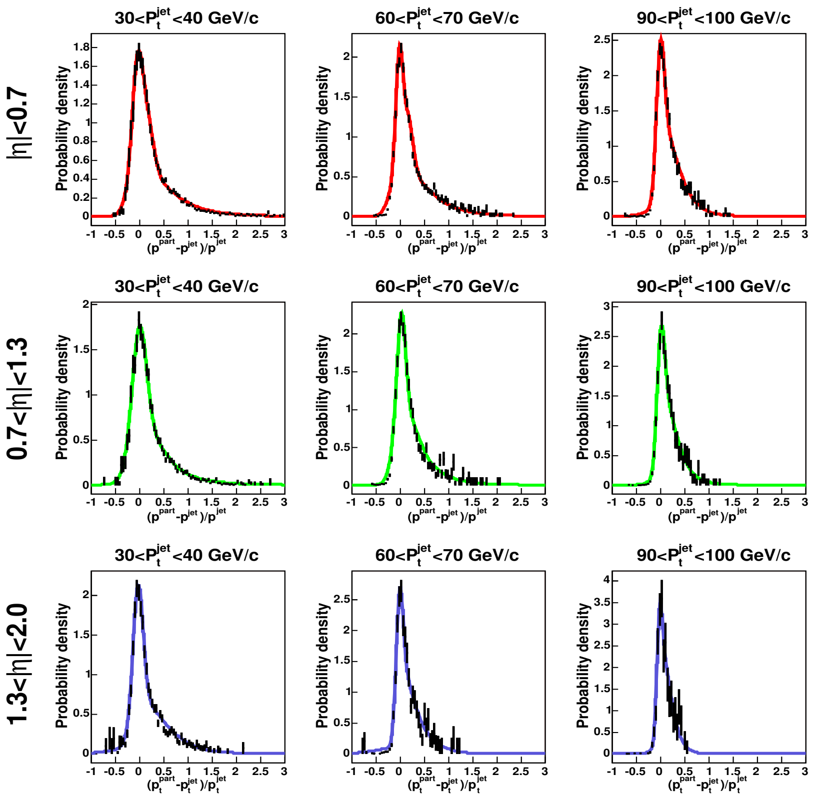

Figure 5: Top Specific Corrections

We used for production of these plots Monte Carlo $t\bar{t}$ events with top mass

[3] also called "top specific corrections"

175, $175 \pm 0.5\ GeV/c^2$. We can assume this trasnfer function can be used through our full analysis because we make them be M_t indipendent (we compansate b parton P_T dependence from M_t by adding an appropriate weight).
We do not see a big difference in respect to the previous analysis [2], as shown in Figure 6: blue dots refer to the procedure of top mass calculation performed

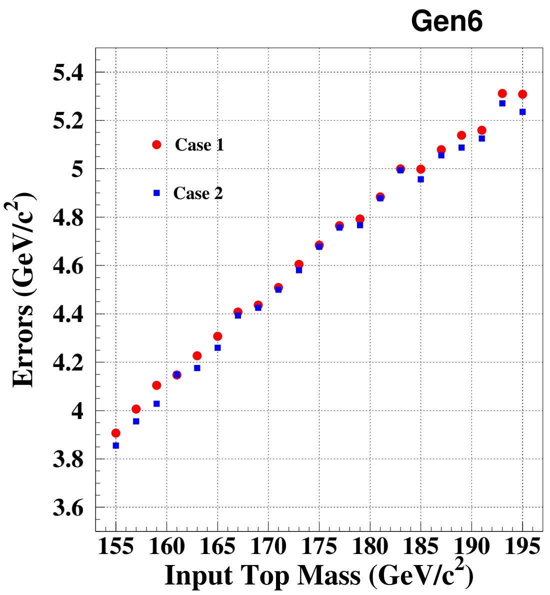

Figure 6: Stastical error improvement by using top specific corrections

by using transfer functions and red ones are for the χ^2 old type i.e. without this transfer functions.

3 Event Selection

The event selection for this analysis is **LTRK** type and performed as described on the Tight Lepton and Isolated Track Sample analyses [7].

For data from periods 8,9,10,11 we used Good Run List v17. This list was modified according to recommendations DQM group conserning to runs with unconsistent beamlines [8]. Selection over data from period 12 were performed with Good Run List v18.

4 Templates

4.1 Monte Carlo Signal Templates

The official MC samples were used. The signal templates for input top masses in the 155÷195 GeV range were created with 2 GeV steps. Then the obtained set of templates was parameterized by one Landau and two Gaussian functions

$$
\begin{aligned}
f_s(M_t^{reco}|M_t) &= p_7 p_6 \frac{1}{\sqrt{2\pi} p_4} e^{-0.5(\frac{M_t^{reco}-p_1}{p_2} + e^{-\frac{M_t^{reco}-p_1}{p_2}})} + \\
&+ (1-p_6)\frac{1}{\sqrt{2\pi} p_5} e^{-0.5(\frac{M_t^{reco}-p_4}{p_5})^2} + (1-p_7)\frac{1}{\sqrt{2\pi} p_3} e^{-0.5(\frac{M_t^{reco}-p_8}{p_3})^2}
\end{aligned}
\tag{15}
$$

Notice that this parametrizing function is strongly dependent from the the input top mass M_t, or it is better to say that its parameters $p_1, \ldots, p_8$, are M_t-dependent.

The examples of our templates are presented in Figs. 7.

4.2 Background template

We used for background processes official Gen.6 MC samples ($WZ \to ll$, $WW \to ll$, $ZZ \to ll$, Drel-Yan, $Z \to \tau\tau$). In order to build general template for Drell-Yan events the templates for each sub-process were combined using their cross-sections and acceptances.

Template for fake events was obtained by weighting the fakeable events from W+jets data sample accoding to the fake rate probability matrix [7].

The obtained templates (Fig. 9) for these processes were combined together according to the expected number of events, as derived by the *ttbar* cross section group [7]; we show these numbers in the Table (see Fig. 8).

Table 1 shows the main components of background and the samples we used to obtain background template. The result for the combined background template is shown in Fig. 9, right lower plot.

The fitting function, f_b, is a slightly bit different from the one used for signal templates, as you can see from the formula (16).

$$
\begin{aligned}
f_b(M_t^{reco}) &= q_7 q_6 \frac{1}{\sqrt{2\pi} q_2} e^{-0.5(\frac{M_t^{reco}-q_1}{q_2} + e^{-\frac{M_t^{reco}-q_1}{q_2}})} + \\
&+ (1-q_6)\frac{1}{\sqrt{2\pi} q_5} e^{-0.5(\frac{M_t^{reco}-q_4}{q_5})^2} + (1-q_7)\frac{1}{\sqrt{2\pi} q_3} e^{-0.5(\frac{M_t^{reco}-q_8}{q_3} + e^{-\frac{M_t^{reco}-q_8}{q_3}})}
\end{aligned}
\tag{16}
$$

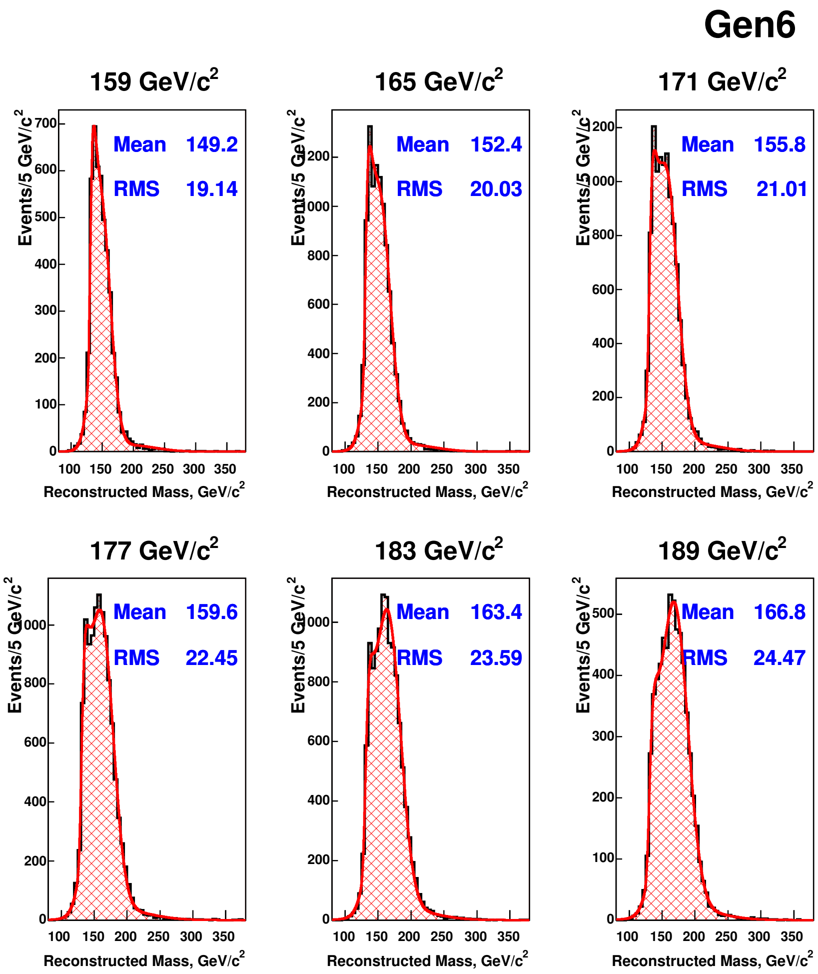

Figure 7: The examples of the signal templates

	$n_j = 0$	$n_j = 1$	$n_j \geq 2$
WW	91.66 ± 7.54	15.96 ± 1.34	3.90 ± 0.36
WZ	10.00 ± 0.83	4.55 ± 0.38	1.43 ± 0.13
ZZ	2.41 ± 0.04	0.65 ± 0.02	0.34 ± 0.02
$Z/\gamma^* \to ee$	72.43 ± 15.79	25.93 ± 6.05	7.75 ± 2.24
$Z/\gamma^* \to \mu\mu$	18.88 ± 5.32	8.88 ± 2.74	3.40 ± 1.15
$Z/\gamma^* \to \tau\tau$	35.54 ± 3.24	26.46 ± 2.47	7.31 ± 0.89
Fakes	244.09 ± 46.41	76.79 ± 14.59	29.85 ± 5.86
Background	475.01 ± 51.58	176.52 ± 16.98	53.99 ± 6.60
$t\bar{t}, \sigma = 6.7$ pb	1.18 ± 0.06	17.29 ± 0.56	60.53 ± 1.88
Predicted	**476.19 ± 31.58**	**176.52 ± 16.98**	**114.51 ± 7.00**
Observed	**443**	**187**	**129**

Figure 8: background numbers from x-section group

Background process	Samples
WW	itopww, wewkbd
WZ	itopwz, wewkcd
ZZ	itopzz
DY	ztop2p, ztopzb, ztop3p, xtop2p, xtoppb, xtop3p, ytop2p, ztop7p, ztopzt, ztop8p, xtop7p, xtoppc, xtop8p, ytop7p, ztopt2, xtopt2, zttt2h
Fakes	W+jets data

Table 1: Samples for background templates.

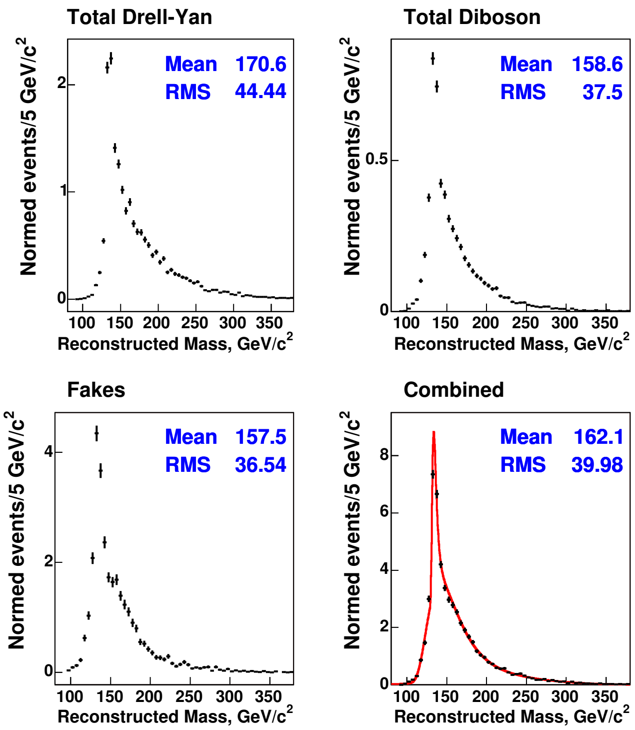

Figure 9: Templates of background processes Drell-Yan, Diboson, “fake” events. Lower right plot shows the combined background.

However, the main difference from f_s is: the f_b parameters $q_1, \ldots, q_8$ are not depend from the top mass.

5 Results from pseudo-experiments

We checked whether the fit with likelihood form (11) was able to return the correct mass by performing the "sanity check" pseudo-experiments for different input top mass values.

According to guidelines [10] the numbers of signal and background events in PE's were Poisson distributed with mean values as their expected numbers. We took as expected numbers 108.95±3.38 and 97.18±11.88 for signal and background respectively. These values were obtained using scaling from 1.1 to 2 fb-1.

The output m$_{top}$ (median of distribution) vs. input M$_{top}$ is shown in Fig. 10. A linear fit yielded a slope of 1.008±0.009. The mean and width of the pull distributions as a function of input top mass are shown in Fig. 11.

The correction for the top mass mean value is 0.16±0.10 GeV/c^2. It is obtained from the fit of the distribution: residual vs. top mass (see Fig. 10).

The obtained correction for pull width is 1.011.

We checked the obtained corrections for top mass value and errors on the set of pseudoexperiments. Results are presented in Figures 12,13.

One can see now that the residual is equal to 0.0 (Fig. 12) and the width of pull distribution is 1.0 (Fig. 13) in the frame of errors.

We estimated the expected statistical error of top quark mass measurement using a MC sample with top mass = $175GeV/c^2$ (see Figure 14). The error is expected to be $4.3GeV/c^2$ and taking into account the pull width correction finally we obtain $4.4GeV/c^2$.

6 Blind test results

Before "opening the box" with data we performed test on the "blind" MC samples. The difference between extracted and true mass values for different "blind" samples in random order are shown in Table 2. The results are good: we have determined the top masses for blind samples with expected accuracy.

We present Figures concerning the "blind" samples here. These are the distriutions of residuals, statistical errors and pull of pseudo-experiments for determination of the "blind top masses" (see Figure 15). The biases for the mean value

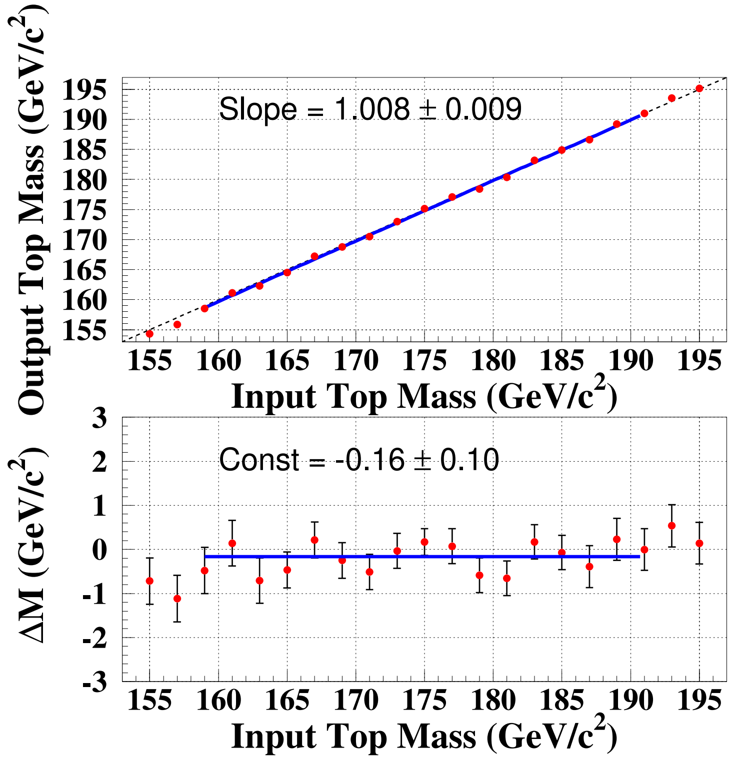

Figure 10: The extracted top mass as a function of input mass. The result of a linear fit is also shown. The lower plot shows the residuals (reconstructed - input top mass).

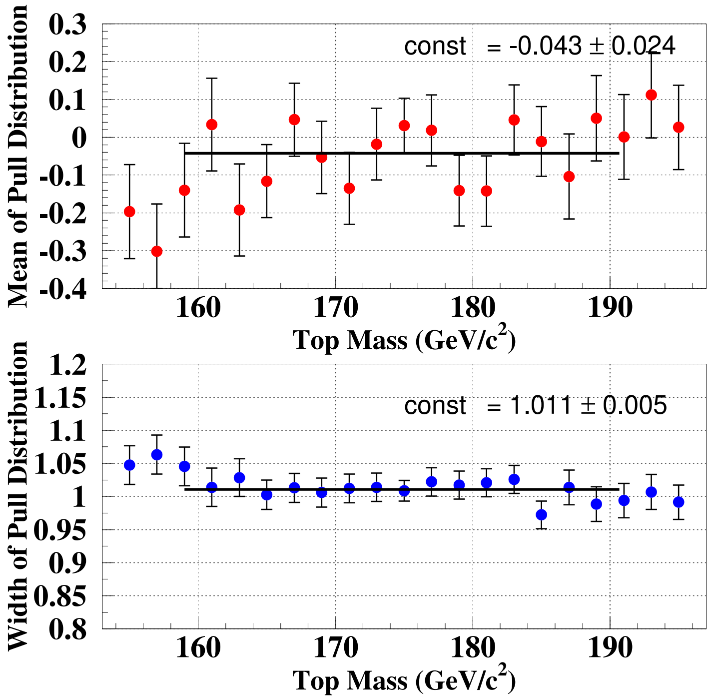

Figure 11: Mean (above) and σ (below) of pull distributions determined from the pseudo-experiments as a function of input top mass.

$M_{rec.}$ - M_{true} (GeV/c^2)	errors	number of sigmas
0.6	1.2	0.5
-0.4	1.2	0.3
1.4	1.2	1.2
-0.9	1.2	0.8
0.3	1.2	0.2
1.4	1.2	1.1
0.3	1.2	0.3
0.0	1.2	0.0
-0.6	1.2	0.5
0.6	1.2	0.5

Table 2: Results on the blind samples

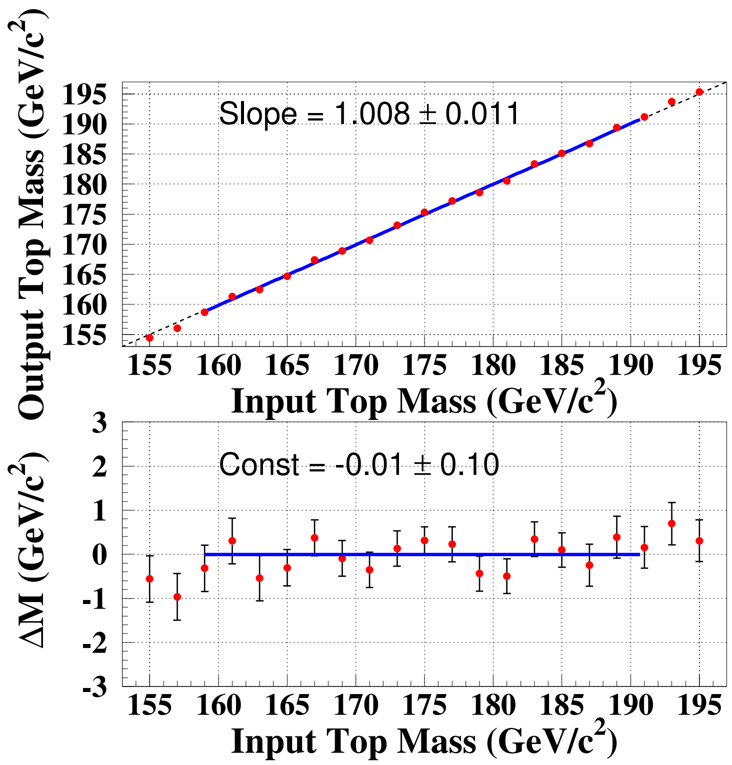

Figure 12: The extracted top mass as a function of input mass after applying the corrections for mean value and for errors. The result of a linear fit is also shown. The lower plot shows the residuals (reconstructed - input top mass).

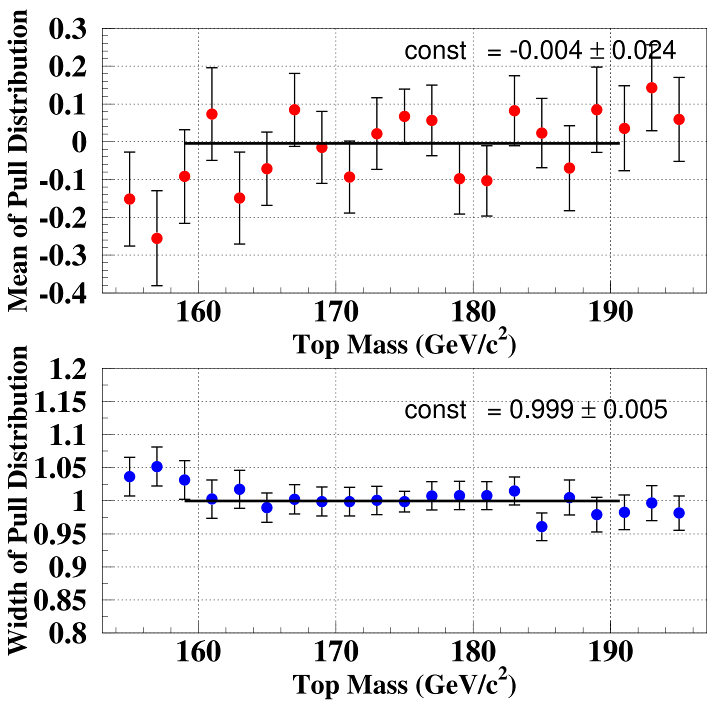

Figure 13: Mean (above) and σ (below) of pull distributions determined from the pseudo-experiments as a function of input top mass. Corrections for mean value and for errors are applied.

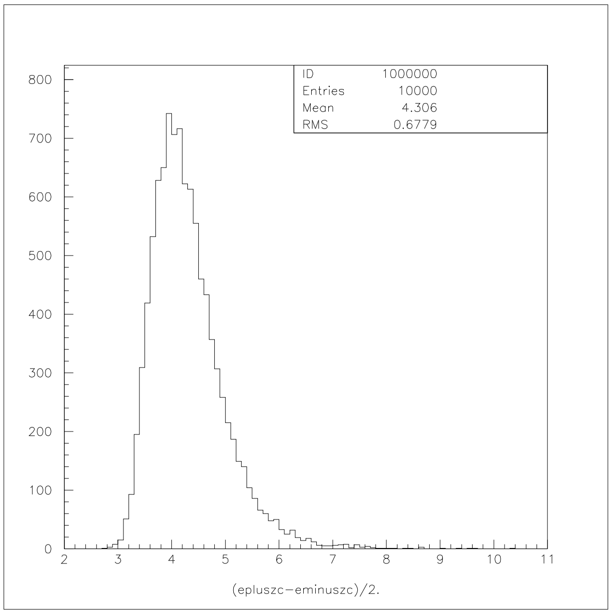

Figure 14: Statistical error distribution for top mass measurement @ MC sample with top mass= $175 GeV/c^2$

(Figure 16) and the pull width (Figure 17) are also presented. We can stress that the bias in pull width conforms to the estimated one: 1.011$\pm$0.005.

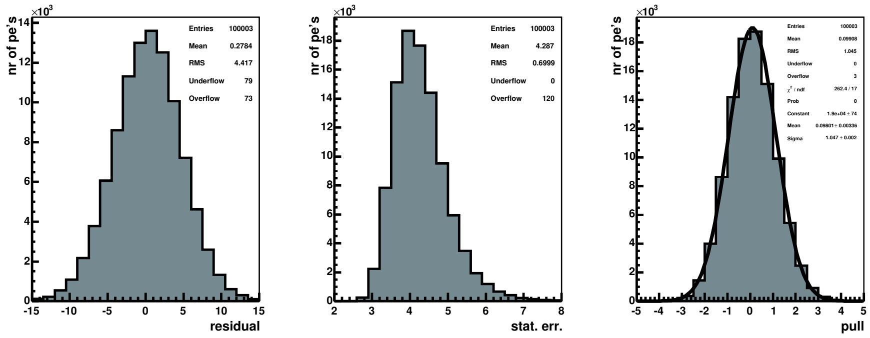

Figure 15: From left to right shown: residuals, statistical errors and pull distribution for pseudo-experiments for determination of the "blind" top masses

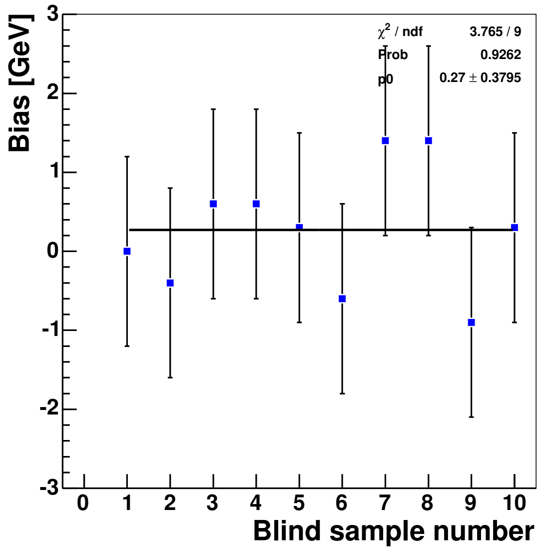

Figure 16: The bias for the blind samples top masses

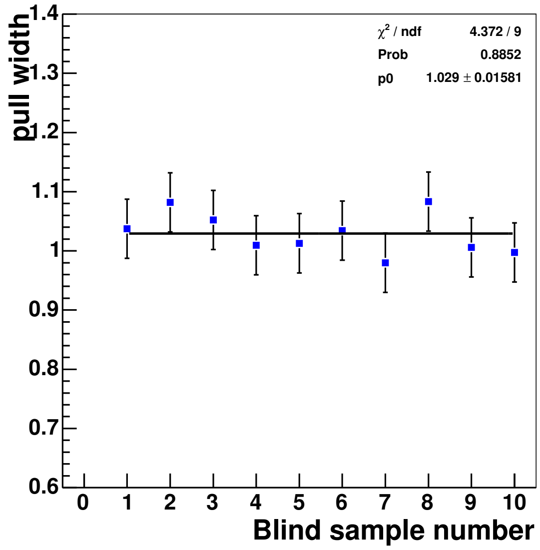

Figure 17: The bias in the pull width for blind samples

7 Systematic Uncertainties

We have considered the following sources of systematic uncertainties on the fitted mass value: a) jet energy scale, b) amount of initial and final state radiation, c) shape of the background template, d) parton distribution functions, and e) approximations made by Monte-Carlo generators, f) b-jet energy scale and lepton energy scale. The magnitudes of these uncertainties were estimated using large Monte-Carlo samples generated only for the systematics study.

The procedure for estimating the systematic uncertainty is similar for all sources. For each source we varied the input value as appropriate (by 1σ, or changing PDF, etc) and evaluated the impact on the returned top mass. This was done by simulating a large number (usually 10000 or more) of pseudo-experiments (PE) with the nominal assumption and with the alternate assumption. The reconstructed mass distribution from each PE was fitted with the same likelihood procedure. The obtained mass value was entered into an ensemble of results of simulated experiments. The systematic uncertainty assigned to our measurement is the difference in the average of these result distributions for the nominal and shifted ensembles or half the difference between results obtained with +sigma and -sigma of the corresponding parameter change.

7.1 Jet Energy Scale

In Run 2 the jet systematic uncertainty is included in the jet correction software package. It is possible to turn on a $\pm\ 1\sigma$ change in the energy scale for the specific type of jet correction. A detailed description of each source of uncertainty can be found at Jet Energy and Resolution Group Web Page [11].

By means of the above-described PE we estimated the mass shift caused by different corrections. We obtained the overall uncertainty of 2.9$\pm$0.03 GeV shifting jets in both signal and background MC events by $\pm\sigma$ of the total jet energy systematic uncertainty.

Individual contributions to the systematic uncertainty are presented in Table 3.

7.2 Radiation Effects, generators and B-jet energy scale

The effects of initial (ISR) and final (FSR) state radiation on the returned top mass were studied using Pythia as a signal generator. To estimate the uncertainty induced by ISR we studied the difference between ISR enhanced and reduced samples, as recommended by the top group. The half-difference between average

Level	Source	M_{rec} (GeV/c^2)		Uncertainty (GeV/c^2)
		$+\sigma$	$-\sigma$	$\Delta M_{rec}/2$
1	η-Dependent	175.80	174.58	0.61 $\pm$0.03
5	Absolute Scale	177.26	172.93	2.17 $\pm$0.03
6	Underlying Event	175.37	175.05	0.16 $\pm$0.03
7	Out-of-cone	176.99	173.36	1.81 $\pm$0.03
	alltogether sources	177.95	172.17	2.88$\pm$0.03
total				**2.88$\pm$0.03**

Table 3: Mass shifts indicated by the PE when the jet energy is shifted by $\pm 1\sigma$ of each separate correction.

reconstructed top masses from these samples are assigned as a systematic uncertainty from ISR. To estimate the uncertainty induced by FSR we used the Pythia with enhanced and with reduced amount of FSR.

The results for the ISR and FSR induced systematic are summarized in Table 4.

The effect of using different top Monte-Carlo generators was checked by comparing nominal Pythia with Herwig samples. The obtained mass shift are presented in Table 4.

Source		Datasets	Mass GeV/c^2	Mass Shift GeV/c^2	Syst. GeV/c^2
B-JES	$\pm$ 1% shift in JES for b-jets	ttkt75(-) ttkt75(+)	174.15$\pm$0.04 176.24$\pm$0.04	$\Delta M/2$ =1.04$\pm$0.03	0.62
Gener.	Herwig Pythia	htop75 ttkt75	174.71$\pm$0.32 175.17$\pm$0.15	ΔM =0.46$\pm$0.35	0.46
ISR	More ISR Less ISR	itoprk itoprl	175.00$\pm$0.32 174.95$\pm$0.32	ΔM =-0.17$\pm$0.34 ΔM =-0.22$\pm$0.34	0.34
FSR	More FSR Less FSR	ftoprj ftoprl	175.05$\pm$0.32 175.38$\pm$0.32	$\Delta M/2$ =0.17$\pm$0.22	0.22

Table 4: Top mass shifts obtained from the PE for different Monte-Carlo samples.

7.3 Background Shape

Background composition.

In order to estimate effect on top mass from the uncertainty in background composition we varied the contribution in combined background template of main sources (Diboson, Drell-Yan and "fakes") by $\pm\sigma$. Contribution from another subsamples was corrected to maintain the total expected number of background events. As result 6 alternative combined background templates were obtained and used for PE's. Obtained top mass shifts presented in Table 5. We assigned 0.46 GeV/c^2 as our systematic error for composition in combined background template.

"Fake" events template shape.
In order to study how the uncertainty for "fake" events template shape can affect our resulting top mass we inserted linear E_T-dependent shift for values in our fake rate matrix. New fake rates were calculated according to the formula:
$w_\pm = w_0 \pm 1/8 \times (2 \times i_{E_T} - 8) \times \sigma_w$
were w_0 is the unshifted fake rate, σ_w is the uncertainty on w_0, and i_{E_T} denotes the E_T bin. Two new fake templates were obtained using changed fake rate matrix and included in combined background template. Using these templates for PE's we got shifts in top mass as presented in Table 5. We took 0.41 GeV/c^2 as our systematic error for uncertainty in template for "fake" events shape.

Drell-Yan template shape.
In order to suppess Drell-Yan events($Z/\gamma^* \to ee, Z/\gamma^* \to \mu\mu$) we have the increased requirement on missing E_T for events with effective mass of lepton and track-lepton inside Z-window (Z-veto cut). Drell-Yan events can get significant value of missing E_T only because mismeasurement of jets E_T. Differencies between modeling of this effect and the reality can give us the shifted top mass. In order to estimate the sensitivity of our measurement to this we insreased (and decreased) by factor of 2 the weight in $Z/\gamma^* \to ee, Z/\gamma^* \to \mu\mu$ templates for events which have effective mass of lepton and track-lepton inside Z-window. Two new combined background templates were obtained using this changed $Z/\gamma^* \to ee, Z/\gamma^* \to \mu\mu$ templates. Then we got from PE's the shifts in the top mass as presented in Table 5. We took 0.3 GeV/c^2 as our systematic error due to uncertainty in Drell-Yan template shape.

7.4 Parton Distribution Functions

The uncertainty induced by PDF's was assessed by comparing CTEQ5L vs MRST in Pythia. The results are listed in Table 6.

The recently developed next-to-leading order PDF from CTEQ6 [12] allows us to vary some PDF sets within their uncertainty. The possible variations are separated into contributions from 20 independent eigenvectors, so in total we have

Source		Mass GeV/c^2	Mass Shift GeV/c^2	Syst. GeV/c^2
BG composition	Diboson(-σ)	175.15±0.04	$\Delta M/2$ =-0.02±0.03	0.03
	Diboson(+σ)	175.11±0.04		
	DY(-σ)	174.90±0.04	$\Delta M/2$ =0.25±0.03	0.25
	DY(+σ)	175.40±0.04		
	Fakes(-σ)	175.53±0.04	$\Delta M/2$ =-0.39±0.03	0.39
	Fakes(+σ)	174.74±0.04		
				0.46
Fake shape	-linear E_T-dependent shift in fake rate matrix	174.80±0.04	$\Delta M/2$ =0.41±0.03	0.41
	+linear E_T-dependent shift in fake matrix	175.61±0.04		
Drell-Yan shape	decreased weight in the Z window	174.88±0.04	$\Delta M/2$ =0.30±0.03	0.30
	increased weight in the Z window	175.48±0.04		

Table 5: Top mass shifts obtained from the PE for different BG composition and fake shape.

41 different sets (1 nominal and 2×20 for $\pm 1\sigma$ variations). The PDF effect is studied using the reweighting method [13], where reconstructed top mass templates for each PDF set are obtained from one single sample (Pythia 175 GeV/c^2 sample) by weighting the mass for each event by the probablity for that event to proceed according to the given PDF. Results for the nominal PDF and for the 20 pairs of $\pm 1\sigma$ PDFs are shown in Fig. 18. The black line corresponds to the nominal PDF set.

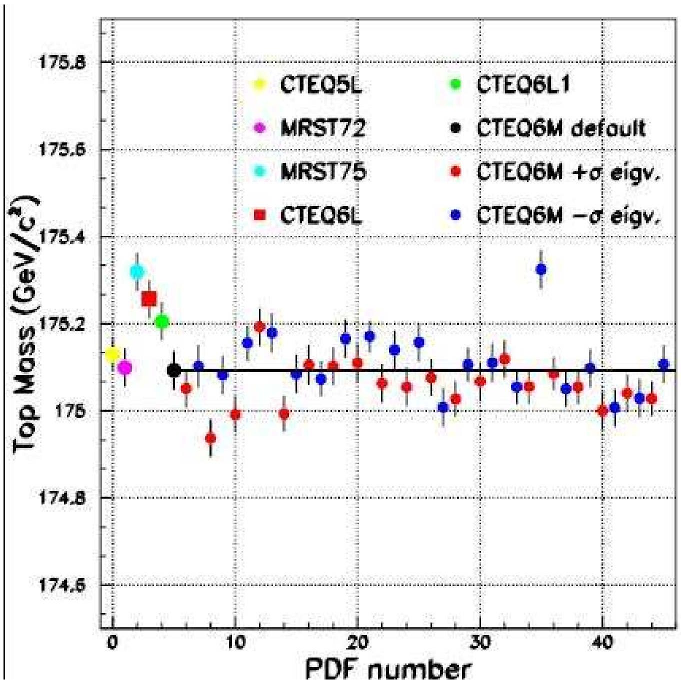

Figure 18: Results used for PDF uncertainty

The total PDF uncertainty was estimated as 0.31 GeV/c^2.

7.5 Lepton energy scale

The effect on the top mass from the uncertanty on lepton energy scale was studied by applying $\pm 1\%$ shifts for lepton p_T [14]. Resulting top mass are 175.48 GeV/c^2 and 174.84 GeV/c^2. We take the half difference (0.3 GeV/c^2) as our systematic error from lepton energy scale uncertainty (see Table 7).

Source	Mass Shift GeV/c^2	Syst. GeV/c^2
CTEQ PDFs	Sum($\Delta M/2$)=0.21$\pm$0.13	0.21
CTEQ5L vs MRST72	ΔM=0.07$\pm$0.06	0.07
α_s (MRST72 vs MRST75)	ΔM=-0.22$\pm$0.06	0.22
Total		0.31

Table 6: PDF Systematic

7.6 Summary of Systematic Errors

The summary of systematic uncertainties are listed in Table 7. For each source of systematic uncertainty we chose the obtained from PE mass shift or its error, which one is bigger.

CDF RunII Preliminary

Source	Uncertainty (GeV/c^2)
Jet Energy Scale	2.9
b-JES	0.6
Initial State Radiation	0.3
Final State Radiation	0.2
Parton Distribution Functions	0.3
Monte-Carlo Generators	0.5
Background composition	0.5
Fakes shape	0.4
DY shape	0.3
l-ES	0.3
Total	**3.1**

Table 7: Symmary of systematic uncertainties

8 Data

The data sample we used in our analysis includes data collected between March 2002 and May 2007 and corresponds to a total integrated luminosity of 2.1 fb^{-1}.

We selected 236 top event candidates. The background was rescaled from track+lepton cross section measurement (1.1 fb^{-1},[7]) and the estimated value is N_b=105.8±12.9.

The two-component, background-constrained fit (N_b=105.8±12.9) for the obtained l+trk sample returns: $M_{top} = 167.57 \pm^{4.15}_{3.99}$ GeV/c^2, with $126.13\pm^{17.99}_{17.41}$ signal events and 108.28±11.5 background events.

The fitted mass distribution is shown in Fig. 19. The insert shows the mass dependence of the negative log-likelihood function.

We also performed a fit when the number of the background events was unconstrained, see Fig. 20. This fit returns $M_{top} = 167.59\pm^{4.42}_{4.21}$ GeV/c^2, with $117.82\pm^{26.48}_{26.59}$ signal events and $118.18\pm^{27.53}_{25.52}$ background events.

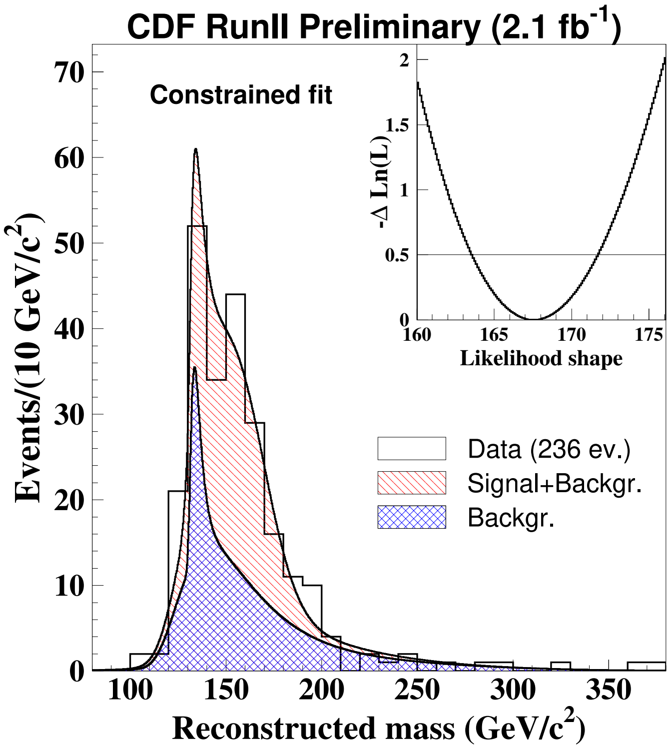

Figure 19: Two-component, constrained fit to the l+trk sample. The violet shaded area corresponds to the background returned by the fit and the red line-shaded area is the sum of background and signal events. The insert shows the mass-dependent negative log-likelihood used in the fit.

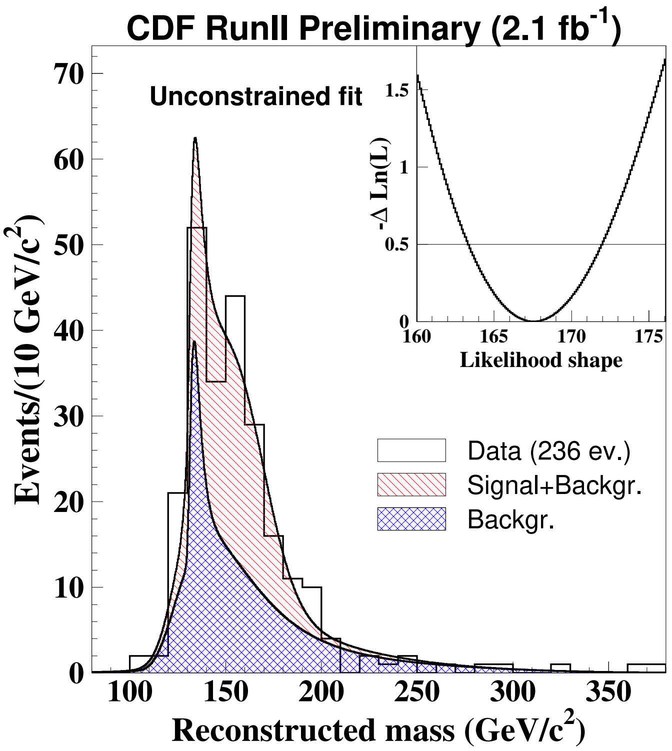

Figure 20: Two-component, unconstrained fit to the l+trk sample. The violet shaded area corresponds to the background returned by the fit and the red line-shaded area is the sum of background and signal events. The insert shows the mass-dependent negative log-likelihood used in the fit.

Expected statistical errors obtained from the pseudoexperiments are shown on Fig 21. The plot shows the stat. error distribution for the top mass of 167 GeV/c^2. The arrows indicate the errors returned by the fit to the data. The probability to have better accuracy then our one from data is 83%.

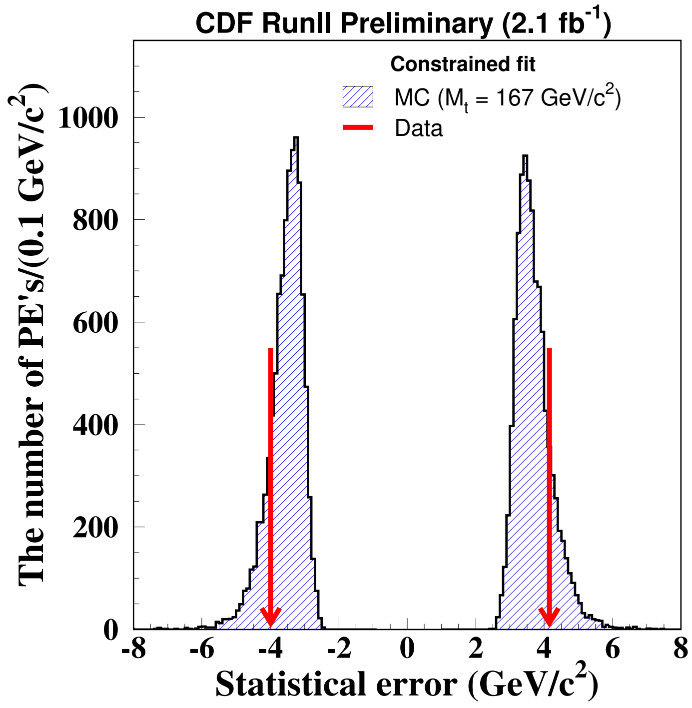

Figure 21: Expected statistical errors for different top masses. The arrows indicate the errors returned by the fit to the data.

9 Conclusion

We applied the neutrino ϕ weighting method to solve a non-constrained kinematics of the top quark decay in dilepton mode.

236 candidate events were selected from the data sample with integrated luminosity of 2.1 fb^-1. Our preliminary measurement of the top quark mass in the l+trk sample is: $M_{top} = 167.73 \pm^{4.2}_{4.03}$ (stat) $\pm$ 3.1 (syst) GeV/c^2. Statistical errors

are shown here after multiplying by factor of 1.011 and the mean value increased on 0.16 GeV/c^2 - the values obtained from our pseudoexperiments.

References

[1] G. Bellettini, J. Budagov, G. Chlachidze, V. Glagolev, F. Prakoshyn, A. Sissakian, I. Suslov, G. Velev. Summer 2004 Top Mass Measurement in Dilepton Events using the MINUIT Fitter *CDF Internal Note 7093*, 2004

[2] G. Bellettini, J. Budagov, G. Chlachidze, V. Glagolev, F. Prakoshyn, A. Sissakian, I. Suslov, G. Velev. Top Mass Measurement in Dilepton Events using Neutrino ϕ Weighting Method. *CDF Internal Note 7641*, 2005

[3] CDF Collaboration, Measurement of the Top Quark Mass using Template Methods on Dilepton Events in Proton-Antiproton Collisions at sqrt(s)=1.96 TeV. *Phys.Rev. D73 (2006) 112006* ,2006.

[4] D. Acosta *et al.* Phys. Rev. D71, 032001 (2005). The CDFII Detector Technical Design Report, Fermilab Report No. Fermilab-Pub-96/390-E.

[5] Gamma vs mtop according Standard Model prediction.

[6] Giorgio Bellettini, Julian Budagov, Guram Chlachidze, Vladimir Glagolev, Fiodar Prakoshyn, Alexei Sissakian, Igor Suslov, George Velev. Measurement of the Top Quark Mass using the Minuit Fitter in Dilepton Events at CDF. *CDF Internal Note 7239*, 2004

[7] J. Thom, J. Incandela, C. Mills, P. Savard, T. Spreitzer. A Measurement of the Top Dilepton Cross-Section using the 1.1 fb^{-1} Tihgt Lepton and Isolated Track Sample. *CDF Internal Note 8696*, 2007

[8] http://www-cdf.fnal.gov/internal/dqm/goodrun/v17/DQM Beamlines.html

[9] T. Maki, J. Antos, A. Beretvas, Y.C. Chen, R. Lysak. Cross-section Dependent Top Mass Measurement in Dileptonic Channel using Template Method. *CDF Internal Note 8823*, 2007

[10] http://www-cdf.fnal.gov/internal/physics/top/run2mass/guidelines.html

[11] Jet Energy and Resolution Group Web Page at http://www-cdf.fnal.gov/internal/physics/top/jets/corrections.html

[12] J.Pumplin et al., “New generation of parton distributions with their uncertainties with global QCD analysis”,hep-ph/0201195

[13] Stephen Miller, http://cdfrh0.grid.umich.edu/ miller/pdf/pdf_acceptance.html, 2004

[14] http://www-cdf.fnal.gov/internal/physics/top/run2mass/sys6.html